



Accelerating changes in ice mass within Greenland, and the ice sheet's sensitivity to atmospheric forcing

Michael Bevis^{a,1}, Christopher Harig^b, Shfaqat A. Khan^c, Abel Brown^a, Frederik J. Simons^d, Michael Willis^e, Xavier Fettweis^f, Michiel R. van den Broeke^g, Finn Bo Madsen^c, Eric Kendrick^a, Dana J. Caccamise II^a, Tonie van Dam^h, Per Knudsen^c, and Thomas Niylenⁱ

^aSchool of Earth Sciences, Ohio State University, Columbus, OH 43210; ^bDepartment of Geosciences, University of Arizona, Tucson, AZ 85721; ^cDTU Space, National Space Institute, Danish Technical University, 2800 Kongens Lyngby, Denmark; ^dDepartment of Geosciences, Princeton University, Princeton, NJ 08544; ^eDepartment of Geological Sciences, University of Colorado, Boulder, CO 80309; ^fDepartment of Geography, University of Liège, 4000 Liège, Belgium; ^gInstitute for Marine and Atmospheric Research, Utrecht University, 3508 TA Utrecht, The Netherlands; ^hFaculty of Sciences, University of Luxembourg, L-4365 Esch-sur-Alzette, Luxembourg; and ⁱUNAVCO, Inc., Boulder, CO 80301

Edited by Mark H. Thiemens, University of California, San Diego, La Jolla, CA, and approved December 14, 2018 (received for review April 17, 2018)

From early 2003 to mid-2013, the total mass of ice in Greenland declined at a progressively increasing rate. In mid-2013, an abrupt reversal occurred, and very little net ice loss occurred in the next 12–18 months. Gravity Recovery and Climate Experiment (GRACE) and global positioning system (GPS) observations reveal that the spatial patterns of the sustained acceleration and the abrupt deceleration in mass loss are similar. The strongest accelerations tracked the phase of the North Atlantic Oscillation (NAO). The negative phase of the NAO enhances summertime warming and insolation while reducing snowfall, especially in west Greenland, driving surface mass balance (SMB) more negative, as illustrated using the regional climate model MAR. The spatial pattern of accelerating mass changes reflects the geography of NAO-driven shifts in atmospheric forcing and the ice sheet's sensitivity to that forcing. We infer that southwest Greenland will become a major future contributor to sea level rise.

GRACE | GNET | NAO | SMB | mass acceleration

The satellite mission Gravity Recovery and Climate Experiment (GRACE) has been used to monitor ice loss in Greenland by inferring near-surface mass changes from temporal variations in gravity measured in space (1–5). Before mid-2013, these measurements were remarkably consistent with a mass trajectory model (6) consisting of an annual cycle, represented by a four-term Fourier series, superimposed on a quadratic or “constant acceleration” trend with an acceleration rate of $-27.7 \pm 4.4 \text{ Gt/y}^2$ (Fig. 1). The Greenland Ice Sheet (GrIS) and its outlying ice caps were losing mass at a rate of about -102 Gt/y in early 2003, but 10.5 y later this rate had increased nearly fourfold to about -393 Gt/y , accounting for much of the observed acceleration in sea level rise (7). Then, from mid-2013 onward, mass loss ceased or nearly ceased (Fig. 1 *B* and *E*) for 12–18 mo. Because seasonally adjusted mass loss stalled, we refer to this time interval as the “2013–2014 Pause” (Fig. 1*B*), or just “Pause.”

The abrupt slowdown in deglaciation was also observed by the Greenland GPS Network (GNET), which senses mass changes by measuring the solid earth's response to changing surface loads (8–12). Vertical crustal displacements manifest a combination of (i) glacial isostatic adjustment (GIA), that is, the solid earth's delayed, viscoelastic response to past changes in ice loads, and (ii) instantaneous, elastic adjustment to contemporary changes in ice mass. GIA rates are nearly constant over decadal and shorter timescales—except, perhaps, near Kangerdlugssuaq Glacier where mantle viscosities are extremely low (11). Therefore, the vertical accelerations frequently observed in GNET displacement time series (6, 8, 12) very largely represent elastic adjustments to accelerating changes in ice mass.

For the 5-y time period of 2008.4–2013.4, which excludes the summer of 2013, our estimates of the mean acceleration in uplift were positive at about 75% of GNET stations, and the largest positive accelerations were nearly three times larger in magnitude

than the most negative accelerations (Fig. 2). In contrast, for the 5-y period of 2010.4–2015.4, which includes the summer of 2013, more than 90% of GNET stations sensed negative accelerations, and the most negative accelerations had nearly three times the magnitude of the most positive accelerations. The ubiquity of the shift in mean vertical acceleration rates can be assessed by comparing the cumulative distribution functions for each time period (Fig. 2*C*). Sign reversal is not strongly sensitive to the limits of these time intervals (see *SI Appendix*, Fig. S2 for another example).

The GRACE time series suggests that the ~ 10 -y episode of accelerating mass loss ceased, and the 2013–2014 Pause in the recent deglaciation of Greenland began near the middle of 2013. Given the level of scatter in the GRACE residuals (Fig. 1*D*), it is hard to be more precise. GNET data provide us with an independent means to estimate the onset time of the Pause. In Fig. 3, we define the station uplift anomalies using a reference period that begins in or after 2007.0 and ends at 2013.4—the final epoch was determined a posteriori, after a series of experiments, so as to establish a self-consistent result. We fit the vertical displacement (up) time series for each GNET station during the reference period with the same trajectory model used to model the GRACE data. This model was then projected forward in time. The uplift anomaly is defined as the difference between the observed

Significance

The recent deglaciation of Greenland is a response to both oceanic and atmospheric forcings. From 2000 to 2010, ice loss was concentrated in the southeast and northwest margins of the ice sheet, in large part due to the increasing discharge of marine-terminating outlet glaciers, emphasizing the importance of oceanic forcing. However, the largest sustained (~ 10 years) acceleration detected by Gravity Recovery and Climate Experiment (GRACE) occurred in southwest Greenland, an area largely devoid of such glaciers. The sustained acceleration and the subsequent, abrupt, and even stronger deceleration were mostly driven by changes in air temperature and solar radiation. Continued atmospheric warming will lead to southwest Greenland becoming a major contributor to sea level rise.

Author contributions: M.B., M.W., F.B.M., D.J.C., and P.K. designed research; M.B., S.A.K., A.B., F.J.S., M.W., X.F., M.R.v.d.B., F.B.M., E.K., D.J.C., T.v.D., and T.N. performed research; M.B. and C.H. analyzed data; M.B. wrote the paper; and F.J.S., X.F., and M.R.v.d.B. helped write the paper.

The authors declare no conflict of interest.

This article is a PNAS Direct Submission.

This open access article is distributed under [Creative Commons Attribution-NonCommercial-NoDerivatives License 4.0 \(CC BY-NC-ND\)](https://creativecommons.org/licenses/by-nc-nd/4.0/).

¹To whom correspondence should be addressed. Email: mbevis@osu.edu.

This article contains supporting information online at www.pnas.org/lookup/suppl/doi:10.1073/pnas.1806562116/-DCSupplemental.

Published online January 22, 2019.

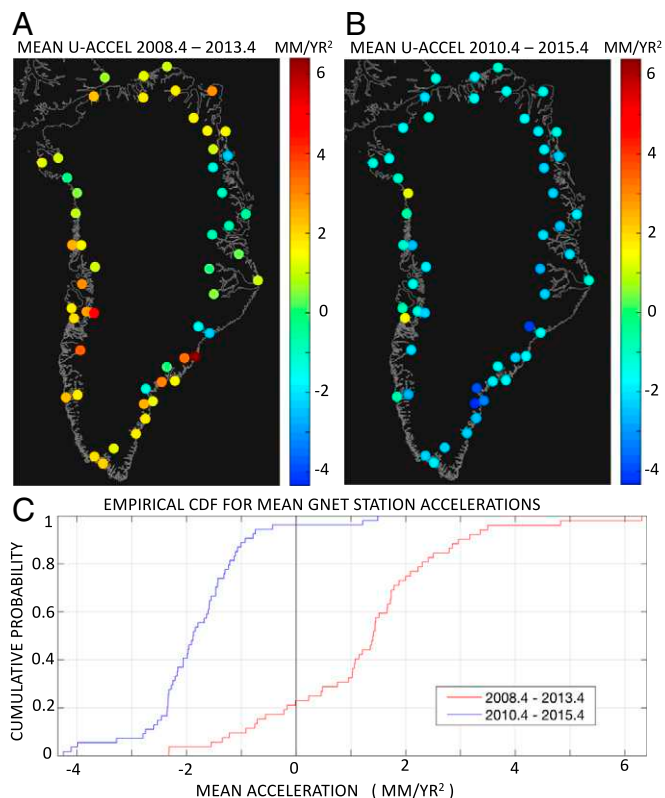


Fig. 2. Mean station accelerations in uplift for two overlapping 5-y time periods. (A) Mean accelerations in the period that began in 2008.4, or when each GNET GPS station was established (if afterward), and ended in 2013.4. (B) The mean accelerations in the time interval 2010.4–2015.4. (C) Empirical cumulative distribution functions (CDFs) for the accelerations in each time period. U-Accel, vertical acceleration.

June to August (JJA) and June to September (JJAS) NAO indices turn positive in 2013, but the change in each of these sNAO indices from 2012 to 2013 was the single biggest interannual change recorded since 1950 (Fig. 1 *F* and *G* and *SI Appendix*, Fig. *S7*). Furthermore, when the sNAO index again turned strongly negative in 2015, significant ice loss was reestablished (Fig. 1 *B* and *E*), and the Pause had ended.

The Spatial Pattern of the Mass Accelerations Recorded by GRACE

We address the spatial structure of the mass accelerations discussed above, by applying the same annual cycle plus quadratic trend model to each cell or “pixel” in our time series of GRACE mass grids. Having fit the composite mass trajectory model to each grid cell in Greenland, we can remove the mean annual cycle, just as we did in Fig. 1*B*, so as to isolate the decycled or seasonally adjusted cumulative mass changes from 2003.12 to 2006.45, 2009.79, or 2013.46 (Fig. 4 *A–C*). The first two subplots (Fig. 4 *A* and *B*) are similar to those of Khan et al. (2) (see their figure 6 *A* and *B*), depicting the spread of ice loss from southeast to northwest Greenland between 2003 and 2009. We also estimated the decycled mass rate as a function of time (Fig. 4 *D–F*), by taking the first temporal derivative of the quadratic mass trend curve. Note the change in sign of mass rate in southwest Greenland between 2003 and 2013.5. In all six subplots of Fig. 4, there is little signal in the central portion of north Greenland, and there is a large segment of the eastern GrIS margin where mass loss and mass rate are much weaker than to the north or south.

The decycled mass acceleration field for the reference period (Fig. 5*A*) is found by taking the second temporal derivative of the

mass trend model. In the event that the mass time series in any given location does not actually have a constant acceleration, then our estimate can be interpreted as the mean acceleration in the time period of interest. The spatial pattern of the GRACE acceleration field is nearly consistent with GNET’s acceleration field (Fig. 2*A* and *SI Appendix*, Fig. *S24*), once we take into account that the elastic responses to mass loss diminish with increasing distance from the centers of ice loss (9, 10, 12). The strongest acceleration in mass loss occurred in and near southwest Greenland (Fig. 5*A*, sector “sw”; *SI Appendix*, section 7). A distinct, smaller, and less intense center of negative mass acceleration is seen in the northeast (Fig. 5*A*, sector “ne”).

We can visualize the mass anomaly associated with the Pause by examining the difference between the projected mass trajectory model and the GRACE solution at epoch 2014.45 (Fig. 5*B*). Alternatively, we can average the mass anomalies in the interval 2013.79–2014.45 just as we did in Fig. 1*D*, but now as a function of position (*SI Appendix*, Fig. *S10*). The two approaches yield similar results. It is instructive to compare the mass anomaly field (Fig. 5*B*), which characterizes the expected mass loss that did not occur (due to the Pause), with the mass acceleration field (Fig. 5*A*) that characterizes mass changes during the previous decade. Apart from a change of sign, the spatial patterns are broadly similar. This strongly suggests that the shifting phase of the NAO (in summer) drove most of the sustained mass acceleration and its abrupt demise. We argue below that the spatial footprint of the sustained acceleration field also reveals the sensitivity of the ice sheet to atmospheric warming, not just the spatial pattern of warming itself.

Even given the unavoidable spatial smoothing of any acceleration field inferred from GRACE, we can conclude that the most negative mass accelerations in Greenland (Fig. 5*A*) occurred in the central west and southwest margins of the GrIS. Shifts in dynamic mass balance (DMB), that is, mass changes driven by changing rates of glacial discharge, at Jakobshavn Isbrae (JI), certainly contributed to the observed mass acceleration in the central west margin before 2006 (ref. 10; *SI Appendix*, section 7). However, further south, there are almost no major marine-terminating glaciers, so the acceleration field in the southwest margin was dominated by SMB, not DMB. This conclusion is supported by model results computed by the regional climate models MAR (15, 16) and

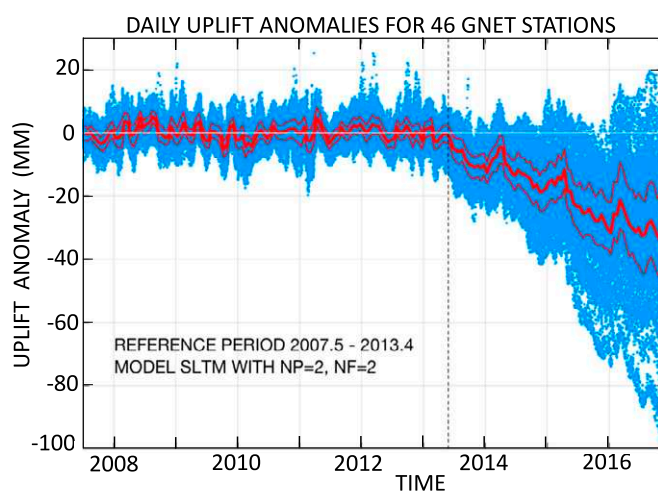


Fig. 3. The combined daily uplift anomalies for 46 GNET stations, and the traveling 25th, 50th, and 75th percentiles of this data cloud. The uplift anomaly is defined as the difference between the observed uplift and a trajectory model consisting of a quadratic trend and a four-term Fourier series fit to all data in a reference period ending in 2013.4. The median anomaly displaces sharply downward at 2013.4 and never returns to zero. NF, # frequencies; NP=2, quadratic trend; SLTM, standard linear trajectory model.

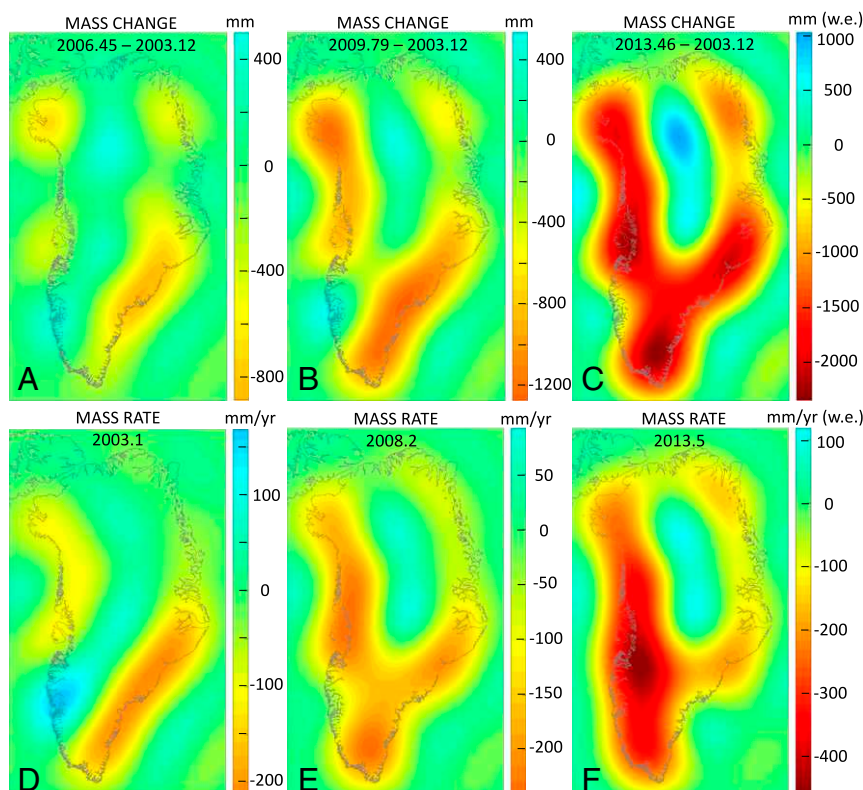


Fig. 4. (A–C) Cumulative mass loss since 2003.12, after the mean seasonal cycle is removed, in millimeters of water equivalent (w.e.), or kilograms per square meter. (D–F) Instantaneous mass rates implied by the quadratic trend model, that is, decycled mass rate, in millimeters per year of water equivalent.

RACMO2 (5). The temporal correlation between summertime SMB and the phase of the NAO is seen in Fig. 1*F*. We estimated the best linear trend in SMB predicted by MAR for the years 2004–2012 (Fig. 5*C*). SMB expressed in water equivalent has units of millimeters per year, so SMB trend has units of millimeters per square year, that is, mass acceleration. The SMB trend field is broadly consistent with the mass acceleration field before 2013, given that the MAR output has much higher resolution (~ 10 km) than GRACE (~ 334 km). GRACE's inevitable blurring of the SMB trend field both broadens the zone of negative mass acceleration in southwest Greenland, and lowers its amplitude. The MAR SMB trend in the northeast GrIS is more pronounced than in adjacent areas, but this local feature is a little less pronounced, and slightly displaced, relative to GRACE's secondary peak in mass acceleration (Fig. 5*A*, “ne”) suggesting that in this area changes in ice dynamics also played a role, as discussed later on. Note that both GRACE and MAR agree on near-zero or slightly positive mass accelerations in the east and southeast margins (Fig. 5*A*, “e” and “se”), respectively. MAR's result for the southeast is associated with positive snowfall anomalies. GNET reveals a slightly more complex situation in which accelerations in uplift rates change sign from one major outlet glacier to the next (Fig. 2*A* and *SI Appendix*, Fig. S24). GRACE tends to smooth out these alternating accelerations in dynamic mass change and blends the result with the more subdued SMB trend due to increased snowfall accumulation.

Topography Modulates the Impact of Atmospheric Warming

The negative phase of the NAO in summertime enhances melting over much of Greenland, but especially in west Greenland (13, 14). The progressive, pre-2013 warming of west Greenland summers was not as spatially focused as the strongest negative mass accelerations (Fig. 5*A* and *C*). The spatial distribution of ablation is largely controlled by the spatial distribution of air temperature and solar

radiation. The ice sheet's sensitivity to surface warming is strongly influenced by surface elevation. If the surface warms from -1 to 3 °C, for example, then the impact of 4 °C warming is vastly greater than if the surface warms from -5 °C to -1 °C. This is why simple models of melting are often expressed in terms of seasonal sums of positive degree-day (17, 18). The amount of melting induced by a temperature increase is strongly dependent on initial surface temperature, and thus on latitude and elevation (*SI Appendix*, Fig. S11), as well as time of year. The influence that surface elevation has on melting and runoff is enhanced by a powerful positive feedback. The ice exposed in the ablation zone has lower albedo than snow surfaces, leading to greater absorption of solar radiation. Indeed, the largest source of melt energy in the ablation zone is absorbed solar energy, not the transfer of sensible heat from the air (19). Nevertheless, the primary control on the geometry of the ablation zone is air temperature, and, at a given time of year, near-surface temperature is largely controlled by latitude and elevation. In a given latitude zone, lower topographic gradients near the margins of the ice sheet lead to a wider ablation zone, thus acting as primary controls on the spatial extent of the albedo feedback.

Even if the southeast and southwest margins of the GrIS were exposed to similar positive temperature trends, the mass loss trend would be more pronounced at the southwest margin because it has a far greater area of low elevation ice surface per unit length of margin than does the southeast margin (Fig. 5*D*). Similarly, the low elevation and surface slopes prevailing at the northeast margin ensure that it incorporates a far greater area of low elevation ice surface than does a similarly sized segment of the northernmost margin of the ice sheet, or a similarly sized segment of the east margin (region “e” in Fig. 5*A*) where surface elevations >2 km loom over the nearby edges of the ice sheet. This helps us explain the localized center of sustained negative mass acceleration in the northeast (Fig. 5*A*, ne). The locally enhanced sensitivity of the

mechanism will be volumetrically concentrated in thinner portions of ice sheet associated with low surface elevations. Meltwater can also accelerate ice flow by modifying the mechanical conditions at the base of the ice sheet (25–27). In extreme cases, the development of subglacial lakes can lift portions of an ice sheet or an ice cap from its bed (28, 29). The hypothesis that atmospheric warming can promote increases in discharge, dynamic thinning, and glacial retreat has recently been invoked in Prudhoe Land in northwest Greenland (30).

Discussion

The coverage and quality of our meteorological, glaciological, and geodetic datasets decline as we regress to the mid-1900s, as does our ability to track the relative importance of SMB and DMB as drivers of deglaciation. Even so, it is clear that the sustained acceleration in mass loss recorded by GRACE before mid-2013 was completely unprecedented (31), as was the collapse of seasonally adjusted mass rate from its peak value to nearly zero in the following 12–18 mo. Mass rate scales with SMB and DMB, so mass acceleration scales with the trend or rate of change of SMB and DMB. Greenland's air–sea–ice system crossed one or more thresholds or tipping points near the beginning of this millennium, triggering more rapid deglaciation. The pronounced negative shift in spatially integrated SMB (Fig. 5E and SI Appendix, Fig. S8) was dominated by increased summertime runoff (Fig. 5E and G). Runoff increased over most of the flanks of the GrIS, but most noticeably in southwest Greenland, where the margin was gaining mass in 2003 but strongly losing mass by late 2012 (Fig. 4). Total glacial discharge integrated over southwest Greenland is not only very low (9.5 ± 1.5 Gt/y) compared with other areas (32), it has been unusually stable as well. South of JI, mass acceleration was dominated by falling SMB from 2000 onward. A little further north, seasonally adjusted discharge rates at JI increased by ~44% from early 2000 to early 2006, but barely changed between early 2006 and early 2012 (32). It was SMB that

was strongly falling in this second 6-y time interval, not DMB (10). Similar considerations apply in southeast Greenland (32).

The decadal acceleration in mass loss in southwest Greenland arose due to the combination of sustained global warming and positive fluctuations in temperature and insolation driven by the NAO. In SI Appendix, we develop an analogy with the global coral bleaching events triggered by every El Niño since that of 1997/1998, but not by any earlier El Niño event. Since 2000, the NAO has worked in concert with global warming to trigger major increases in summertime runoff. Before 2000, the air was too cool for the NAO to do the same. In a decade or two, global warming will be able to drive 2012 levels of runoff with little or no assistance from the NAO. In the shorter term, we can infer that the next time NAO turns strongly negative, SMB will trend strongly negative over west and especially southwest Greenland, just as future warming of the shallow ocean is expected to have its largest impact, via DMB (33, 34), in southeast and northwest Greenland. Because ice sheet topography equips southwest Greenland with greater sensitivity to atmospheric forcing, we infer that within two decades this part of the GrIS will become a major contributor to sea level rise. There is also the suggestion that enhanced summertime melting may induce more sustained increases in discharge rates.

Materials and Methods

We used the global GRACE solution CSR release RL-05. Our regional GRACE analysis used the methodology of ref. 3. Our GPS data processing followed that of ref. 6, as did our approach to time series analysis, both for GRACE and GNET. We characterized SMB in Greenland using the regional climate models MAR (15) and RACMO2 (5). Further details, and a discussion of data access, can be found in SI Appendix.

ACKNOWLEDGMENTS. We thank Robin Abbot of Polar Field Services for her unflinching logistical support. We are grateful to two anonymous reviewers for their comments and suggestions. This research and GNET were supported by National Science Foundation Grant PLR-1111882.

- Velicogna I, Wahr J (2006) Acceleration of Greenland ice mass loss in spring 2004. *Nature* 443:329–331.
- Khan SA, Wahr J, Bevis M, Velicogna I, Kendrick E (2010) Spread of ice mass loss into northwest Greenland observed by GRACE and GPS. *Geophys Res Lett* 37:L06501.
- Harig C, Simons FJ (2012) Mapping Greenland's mass loss in space and time. *Proc Natl Acad Sci USA* 109:19934–19937.
- Wouters B, et al. (2014) GRACE, time-varying gravity, Earth system dynamics and climate change. *Rep Prog Phys* 77:116801.
- Van den Broeke MR, et al. (2016) On the recent contribution of the Greenland ice sheet to sea level change. *Cryosphere* 10:1933–1946.
- Bevis M, Brown A (2014) Trajectory models and reference frames for crustal motion geodesy. *J Geod* 88:283–311.
- Chen X, et al. (2017) The increasing rate of global mean sea-level rise during 1993–2014. *Nat Clim Change* 7:492–495.
- Bevis M, et al. (2012) Bedrock displacements on Greenland driven by ice mass variations, climate cycles and climate change. *Proc Natl Acad Sci USA* 109:11944–11948.
- Nielsen K, et al. (2012) Crustal uplift due to ice mass variability on Upernavik Isstrom, west Greenland. *Earth Planet Sci Lett* 353-354:182–189.
- Nielsen K, et al. (2013) Vertical and horizontal surface displacements near Jakobshavn Isbrea driven by melt-induced and dynamic ice loss. *J Geophys Res* 118:1–8.
- Khan SA, et al. (2016) Geodetic measurements reveal similarities between post-Last Glacial Maximum and present-day mass loss from the Greenland ice sheet. *Sci Adv* 2: e1600931.
- Khan SA, et al. (2014) Sustained mass loss of the northeast Greenland ice sheet triggered by regional warming. *Nat Clim Change* 4:292–299.
- Van Angelen J, et al. (2014) Contemporary (1960–2012) evolution of the climate and surface mass balance of the Greenland ice sheet. *Surv Geophys* 35:1155–1174.
- Fettweis X, et al. (2013) Brief communication "Important role of the mid-tropospheric atmospheric circulation in the recent surface melt increase over the Greenland ice sheet." *Cryosphere* 7:241–248.
- Fettweis X, et al. (2013) Estimating the Greenland ice sheet surface mass balance contribution to future sea level rise using the regional atmospheric climate model MAR. *Cryosphere* 7:469–489.
- Fettweis X, et al. (2017) Reconstructions of the 1900–2015 Greenland ice sheet surface mass balance using the regional climate MAR model. *Cryosphere* 11:1015–1033.
- Brathwaite R (1995) Positive degree-day factors for ablation on the Greenland ice sheet studied by energy-balance modeling. *J Glaciol* 41:153–160.
- Lecavalier B, et al. (2014) A model of Greenland ice sheet deglaciation constrained by observations of relative sea level and ice extent. *Quat Sci Rev* 102:54–84.
- Van den Broeke MR, Smeets C, van de Wal R (2011) The seasonal cycle and inter-annual variability of surface energy balance and melt in the ablation zone of the west Greenland ice sheet. *Cryosphere* 5:377–390.
- Ahlström AP, Petersen D, Langen PL, Citterio M, Box JE (2017) Abrupt shift in the observed runoff from the southwestern Greenland ice sheet. *Sci Adv* 3:e1701169.
- Tedesco M, et al. (2016) Arctic cut-off high drives the poleward shift of a new Greenland melting record. *Nat Commun* 7:11723.
- Wendt J, et al. (2010) Recent ice-surface-elevation changes of Fleming Glacier in response to the removal of the Wordie Ice Shelf, Antarctic Peninsula. *Ann Glaciol* 51: 97–102.
- Rott H, Müller F, Nagler T, Floricioiu D (2011) The imbalance of glaciers after disintegration of Larsen-B ice shelf, Antarctic Peninsula. *Cryosphere* 5:125–134.
- Phillips T, Rajaram H, Colgan W, Steffen K, Abdalati W (2013) Evaluation of cryo-hydrologic warming as an explanation for increased ice velocities in the wet snow zone, Sermeq Avannarleg, West Greenland. *J Geophys Res* 118:1241–1256.
- Parizek BR, Alley RB (2004) Implications of increased Greenland surface melt under global-warming scenarios: Ice-sheet simulations. *Quat Sci Rev* 23:1013–1027.
- Schoof C (2010) Ice-sheet acceleration driven by melt supply variability. *Nature* 468: 803–806.
- Bartholomew I, et al. (2012) Short-term variability in Greenland ice sheet motion forced by time-varying meltwater drainage: Implications for the relationship between subglacial drainage system behavior and ice velocity. *J Geophys Res* 117:F03002.
- Das SB, et al. (2008) Fracture propagation to the base of the Greenland ice sheet during supraglacial lake drainage. *Science* 320:778–781.
- Willis MJ, Herried BG, Bevis MG, Bell RE (2015) Recharge of a subglacial lake by surface meltwater in northeast Greenland. *Nature* 518:223–227.
- Sakakibara D, Sugiyama S (2018) Ice front and flow speed variations of marine-terminating outlet glaciers along the coast of Prudhoe Land, northwestern Greenland. *J Glaciol* 64:300–310.
- Khan SA, et al. (2015) Greenland ice sheet mass balance: A review. *Rep Prog Phys* 78: 046801.
- King M, et al. (2018) Seasonal to decadal variability in ice discharge from the Greenland ice sheet. *Cryosphere* 12:3813–3825.
- Holland D, Thomas R, De Young B, Ribergaard M, Lyberth B (2008) Acceleration of Jakobshavn Isbrea triggered by warm subsurface ocean waters. *Nat Geosci* 1:659–664.
- Straneo F, Heimbach P (2013) North Atlantic warming and the retreat of Greenland's outlet glaciers. *Nature* 504:36–43.

Supporting Information (SA) Appendix

Accelerating changes in ice mass within Greenland, and the ice sheet's sensitivity to atmospheric forcing

M. Bevis et al.

1. GRACE analysis

We used a time series of near-surface mass change fields derived from the Center for Space Research (CSR) GRACE release RL-05 products. We spatially analyze the GRACE data by projecting the global spherical harmonic solutions into a local basis of scalar spherical Slepian functions. This basis isolates mass changes in the immediate vicinity of Greenland while minimizing the influence of signal and noise that occur in other parts of the world (Harig and Simons, 2012). We evaluate these mass fields on a grid that preserves the spatial resolution of the original CSR solution (~ 334 km). We also spatially integrate these mass fields across Greenland so as to characterize temporal changes in the mass of the entire ice sheet and any outlying ice caps and land-based glaciers. Both the total mass time series, and the mass time series for each grid point, are analyzed in the time domain using a standard linear trajectory model (SLTM) (6) consisting of an annual cycle represented by a 4-term Fourier series, and a quadratic or 'constant acceleration' trend. This model was fit to all the observations prior until mid 2013 (before the Pause began), and projected forward in time. Mass anomalies are defined as the difference between the observations and the model.

Although the cyclical component of the SLTM in Fig. 1a has constant amplitude and constant phase (see the dashed black curve in **Fig. S1**) it interacts with the increasing negative slope of the trend component of the SLTM (the dashed red line in Fig. 1a) to produce an increasing asymmetry to the inter-annual mass change curves from one year to the next, as seen in the solid curves in Fig. S1, which are color-coded by year.

The low amplitude positive acceleration peak (Fig. 5a) observed just offshore of SE Greenland is rather enigmatic. It might be caused by shifting patterns of ocean circulation, but the absence of similar accelerations in the oceans near other coastal sectors argues against this interpretation. It may just result from 'ringing' of the model acceleration surface driven by the much larger negative peak near the SW margin.

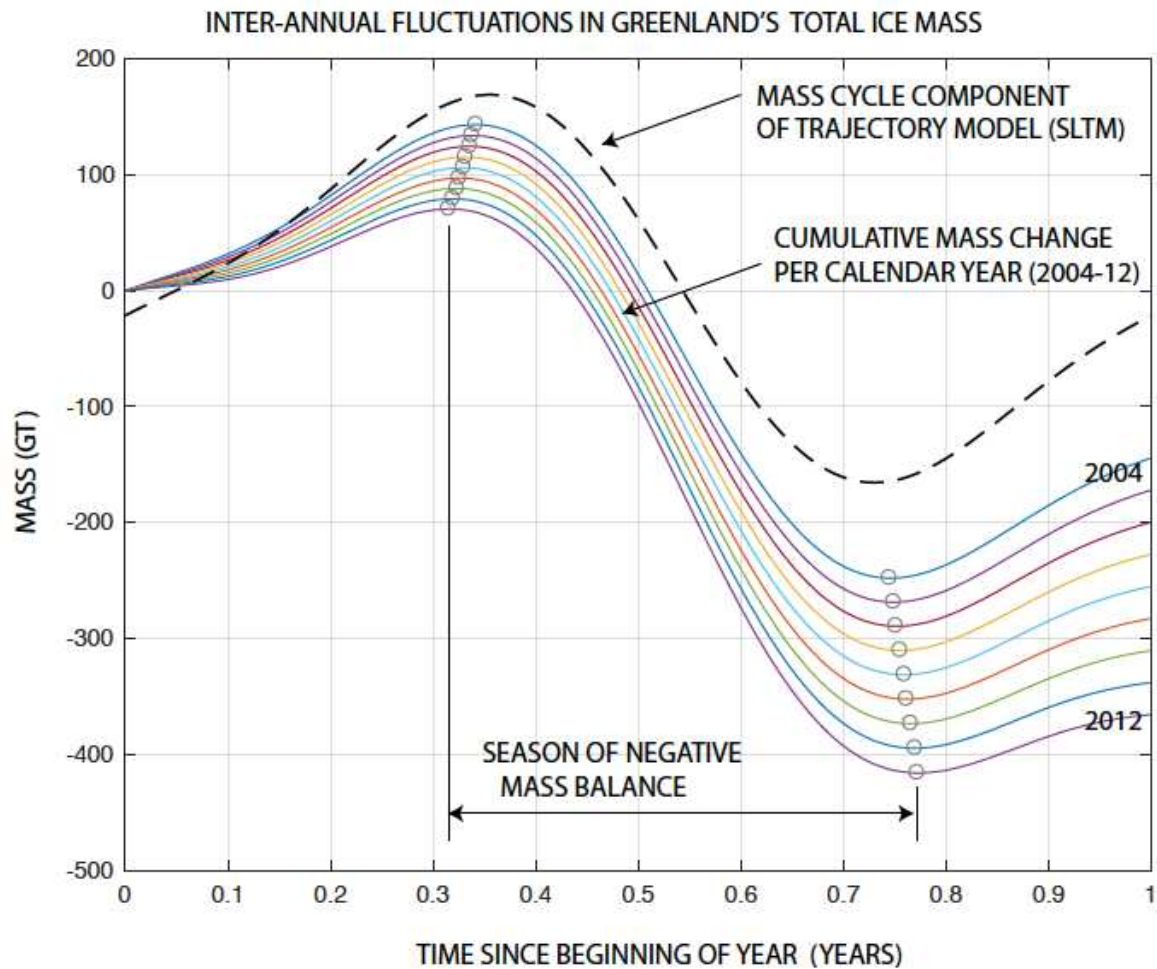


Figure S1. The dashed line represents the cyclical component of the SLTM used to model the GRACE mass trajectory, which is also seen in Fig. 1c. When this pure cycle is added to a quadratic (constant acceleration) trend curve (Fig. 1a,b) interacts with the cycle to produce an increasingly asymmetrical intra-annual mass variation curve. These intra-annual mass change curves are shown by the solid colored curves, starting with 2004 and ending with 2012, the last complete curve before the Pause. The total range of mass variation increases from one year to the next, and the annual peaks and troughs of these curves (open circles), which mark the beginning and end of the season of mass loss, shift in opposite directions. This means that the season of negative mass balance got longer with each passing year, and so did the mass loss in that season. In contrast, the season of mass growth got shorter each year, and the mass gain within that season diminished from one year to the next.

2. GPS data processing.

The daily GNET data processing was performed using MIT's GAMIT/GLOBK software, as part of a much larger global analysis comprising about 3.4 million station-days of observations. The stacking of the daily polyhedra, the imposition of the reference frame, and the estimation of the station trajectory models was performed using the OSU software TSTACK. The workflow and analysis protocols have been described by refs (6, 8) and Bevis et al. (2012).

3. GNET's mean vertical acceleration as a function of time window

To compute the accelerations shown in Figure 3, we fit vertical displacement time series observed at a large set of GNET stations with a SLTM in which the component trend model is quadratic in time, and therefore invokes constant acceleration. The estimated acceleration is twice the value of the coefficient associated with the term $(t - t_R)^2$ where t is time and t_R is the reference time. If the acceleration rate actually varies in time within the time window of the analysis, we interpret the estimated acceleration as the mean acceleration in the time window. Thus Fig. 3a and 3b compare the mean accelerations in two overlapping time windows, both 5 years wide. It is also interesting to examine the mean acceleration between the start of 2007 and mid 2013 and contrast it with the mean acceleration for the period 2007–2015.4 (**Fig. S2**). Many GNET stations were constructed in the summer of 2007, but GNET was not completed until early September 2009. So, the acceleration maps in Fig. S2 are a little harder to interpret than those in Fig. 2 because the time series used to make Fig. S2 have a much wider scatter in starting times, and therefore in time window length. (See Fig. S2 in the Supporting Information appendix of Bevis et al. (2012) to determine the year in which any GNET station first became operational). But even so, it is extraordinary that extending the time window from 2007 to 2015.4 causes the mean acceleration rates to flip sign at about $\frac{3}{4}$ of all GNET stations (Fig S2 c). This clearly implies that a huge deceleration in mass loss occurred between 2013.4 and 2015.4, over Greenland as a whole.

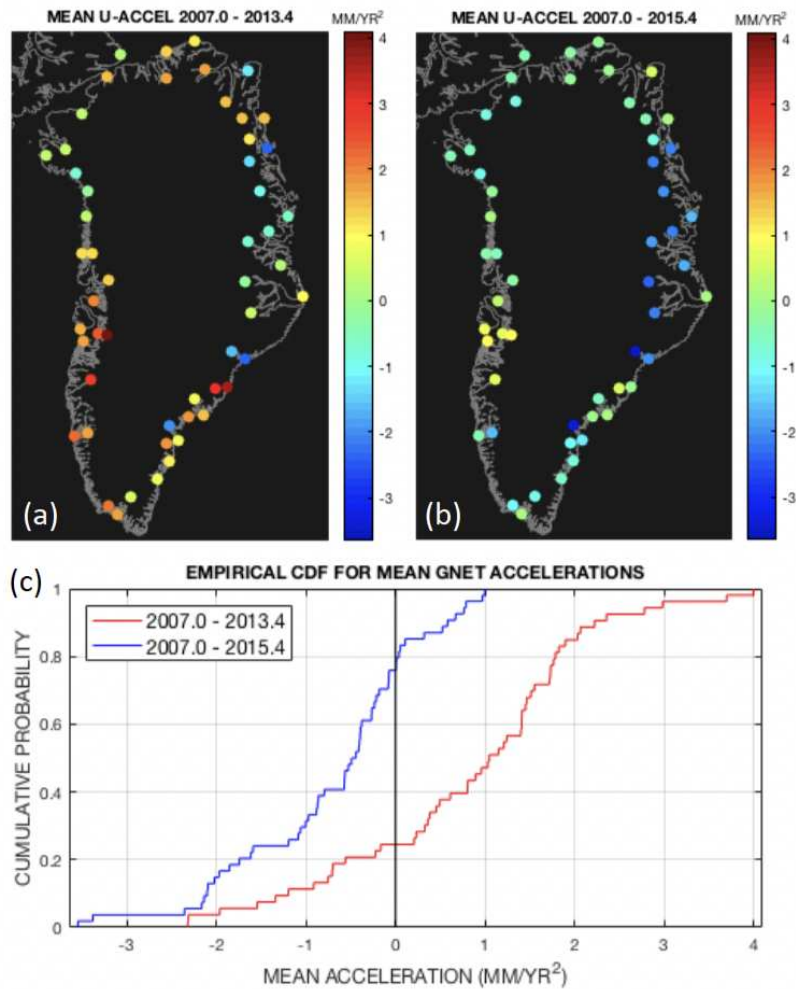


Figure S2. Contrasting the mean acceleration levels (after the mean annual acceleration cycle is removed), using the same methodology as that used to obtain the results in Fig. 3. (a) The mean accelerations in the period that began at the start of 2007, or when each GPS station was established if that was afterwards, and ended in 2013.4. (b) The mean accelerations for the time interval that started in 2007.0, or when the GPS station started if that was later, and 2015.4. (c) The empirical CDF functions for the acceleration estimates in both time periods. Note that the time interval for (a) is a large subset of the time interval for (b), implying that a major deceleration occurred over most of GNET between 2013.4 and 2015.4.

4. Use of GNET to estimate the onset time of the ‘2013-2014 Pause’

The result shown in Fig. 2 is insensitive to the precise end time assigned to the reference period. Indeed, we show here that even if we abandon the prior assumption of a quadratic trend in the reference period, and simply de-cycle (or seasonally adjust) the vertical displacement time series, and then remove the best fit linear trend prior to some epoch close to mid-2013, we still find a collective change of trend beginning close to 2013.4 (**Fig. S3**).

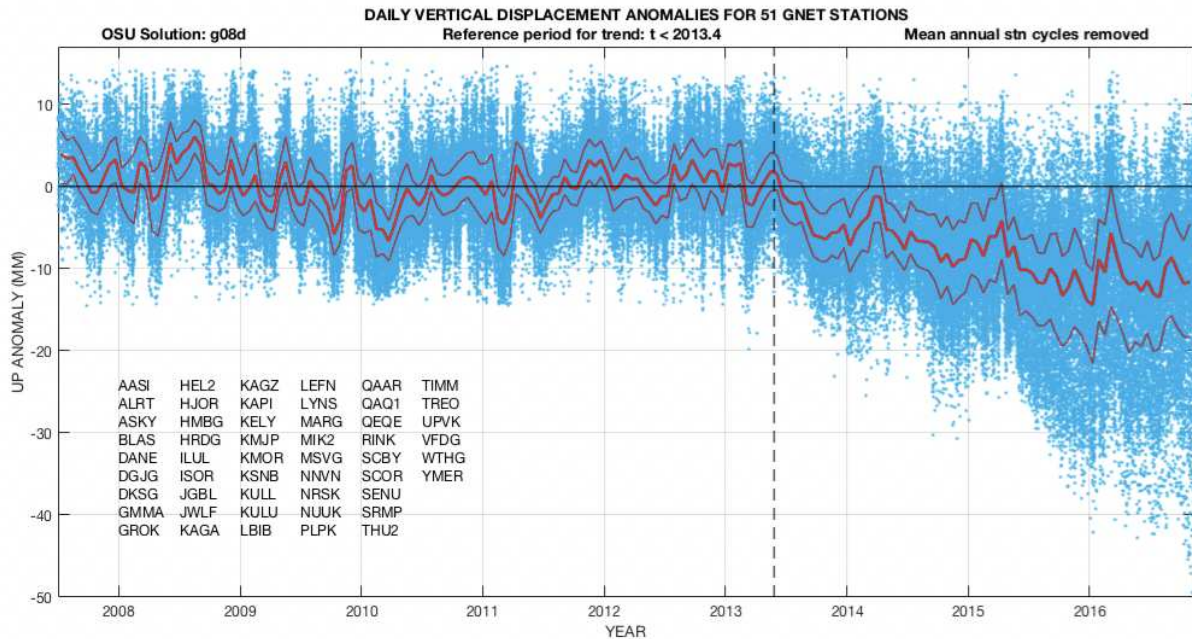


Figure S3. The de-cycled and de-trended displacement time series for 51 GNET stations (blue dots) from 2007.5 to late 2016, obtained by removing the mean annual cycle and the best-fit linear trend estimated in the reference period ending in 2013.4. The red curves represent the 25th, 50th and 75th percentile obtained using a travelling window with a width of 0.1 years. Note that unlike the curves in Fig. 3, the curves tend to be positive at the beginning of the reference window, negative in the middle, and positive near the end of the window. This curvature reflects the presence of a sustained acceleration in the reference period, which was accounted for in SLTM of Fig. 3, but which has been ignored in this analysis. Even so, the median curve deflects downwards and then remains negative shortly after 2013.4, providing evidence that the result obtained in Fig.3 is rather robust.

It is also possible to see the cessation of uplift associated with the Pause in deglaciation in the raw geodetic time series at many GNET stations (**Fig. S4**), though it is usually easier to assess the time the Pause begins at a given station by viewing its uplift anomaly time series (**Fig. S5**). Khan et al. (2014) have already discussed the accelerating rates of uplift observed at the GNET stations in NE Greenland prior to the summer of 2013, and here we show (**Fig. S6**) the cessation of uplift during the following year.

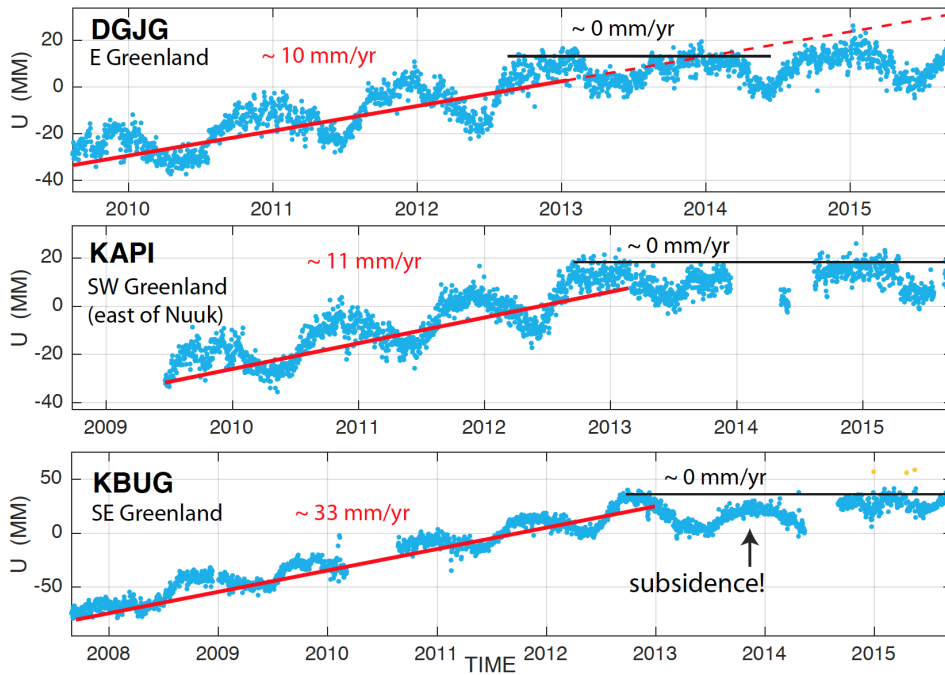


Figure S4. The raw vertical time series $U(t)$ at two GNET stations, DGJG and KAPI, showing consistent uplift prior to 2013.4 and a subsequent pause in uplift that lasted between one and two years. The behavior at KBUG was anomalous in that dynamic changes in two nearby outlets of Koge Bugt glacier caused the ground to begin subsiding in very late 2012 or very early 2013, rather than around 2013.4. The only other GNET station sharing this behavior is the neighboring station TREO, where wintertime DMB changes associated with an adjacent glacier preceded and then superimposed on the regional SMB anomaly responsible for the Pause. As seen in Fig. S5, it is easier to assess the onset of the Pause near any given GNET station by examining the uplift anomaly time series.

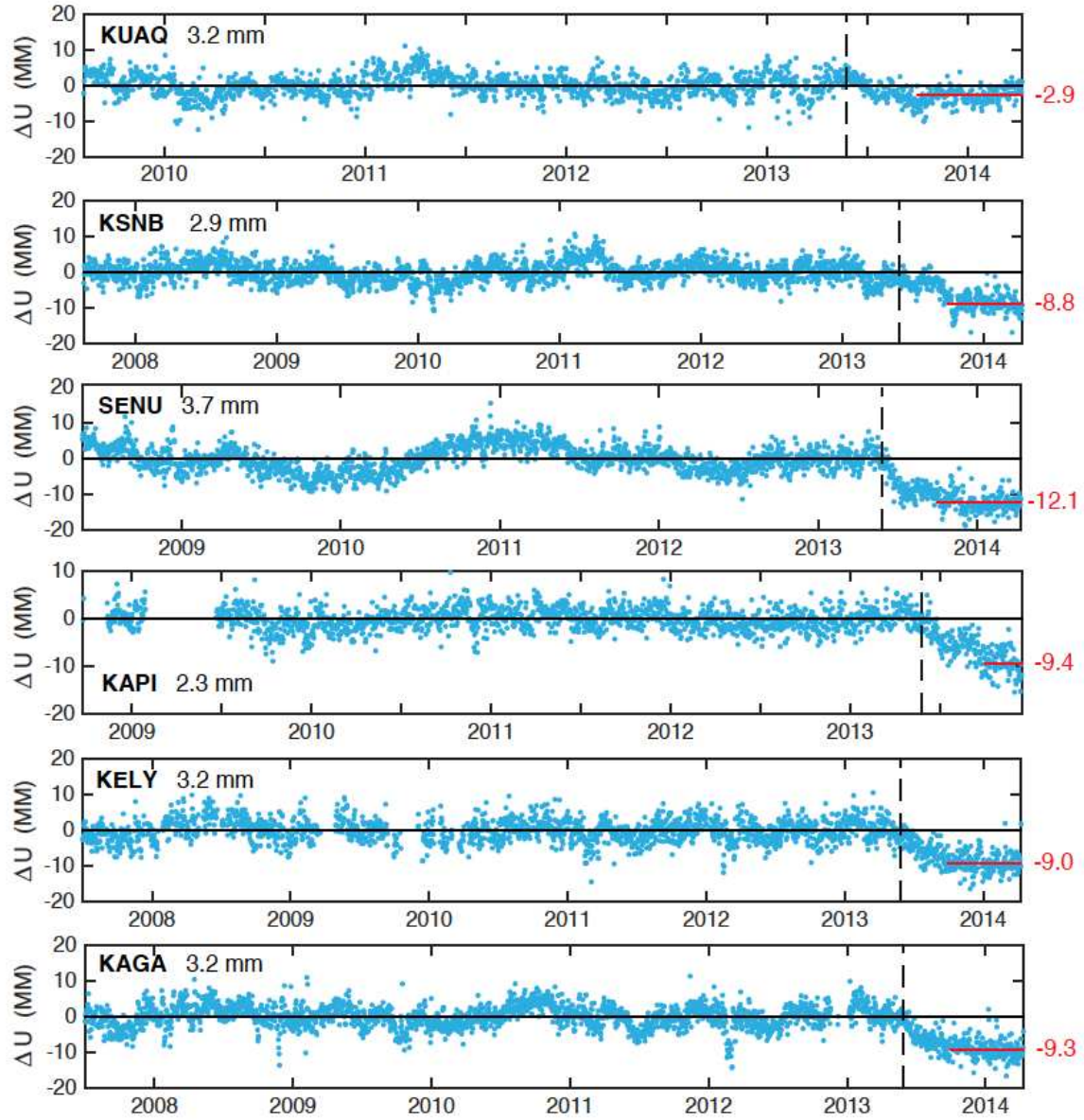


Figure S5. The uplift anomalies observed at 6 GNET stations located in Central and Southern Greenland. The number shown next to the station code is the WRMS scatter during the reference period, which terminates at 2013.4 (dashed vertical line). Note that the onset of the negative displacement anomaly at each station -- constituting the beginning of the Pause -- starts at or shortly after 2013.4. Contrast this with the situation in NE Greenland (Fig. S6).

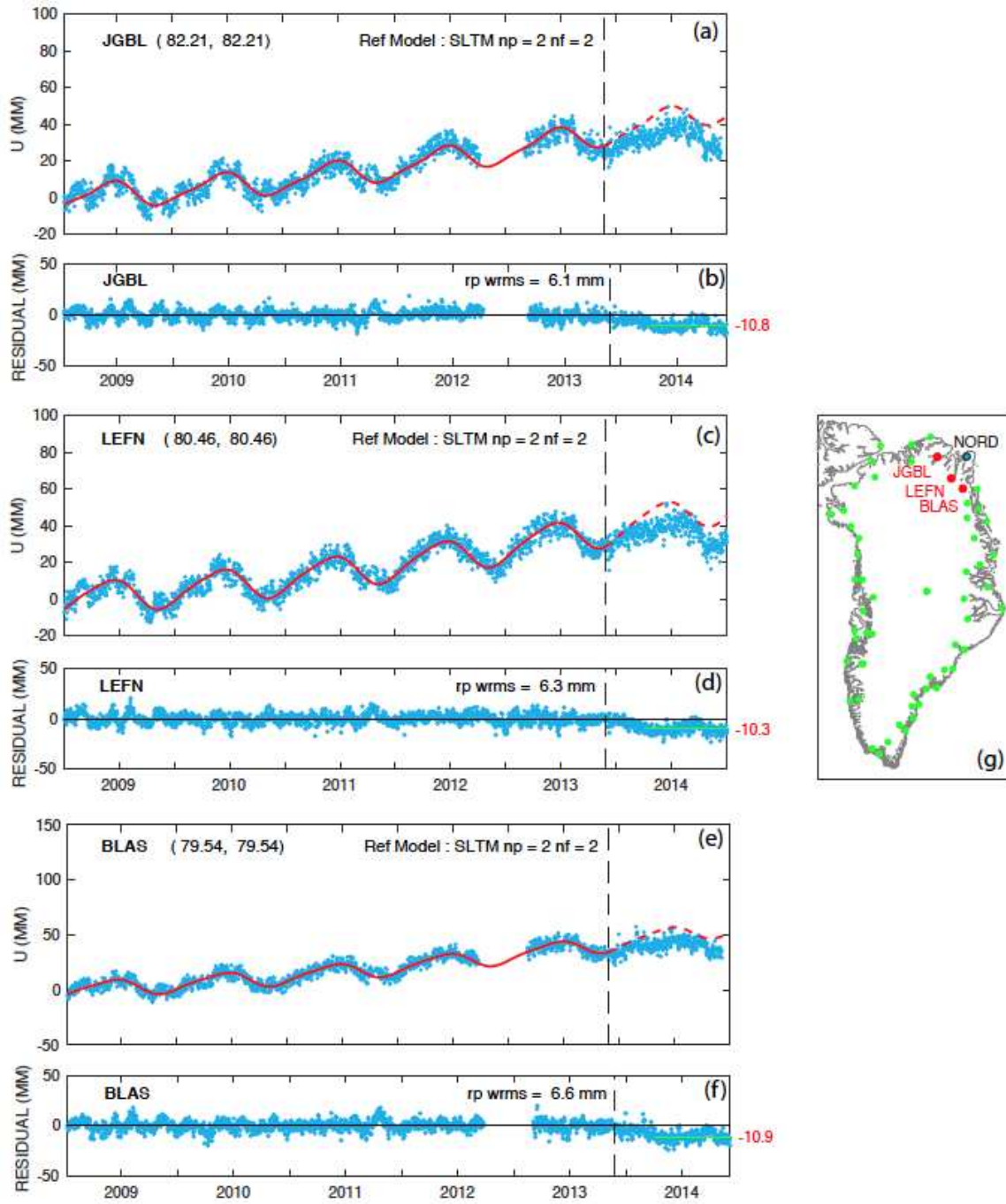


Figure S6. The uplift histories at GNET stations (a) JGBL, (c) LEFN and (e) BLAS, plus the trajectory models fit to the daily observations (blue dots) prior to 2013.4 (red curves), and the associated uplift residual time series in subplots (b), (d) and (f). The station locations are shown by red dots in map (g). Note that the anomalies shift systematically downwards later than the median onset time 2013.4, largely because the summer melting season starts later in NE Greenland than it does at most GNET locations.

5. Summertime NAO indices

Summertime NAO indices were obtained by averaging NOAA’s monthly listings, which extend back to 1950. They can be found at this URL:

<http://www.cpc.ncep.noaa.gov/products/precip/CWlink/pna/nao.shtml>

We chose to average the values for June–September (JJAS) to represent ‘summertime’, rather than the more conventional choice of June–August (JJA), because ‘summertime’ temperatures clearly persisted into September during the summer of 2012 (Van Angelen et al., 2014).

However, if we use the NAO JJA index instead (**Fig. S7**), the results are little different than those seen in Fig. 1f

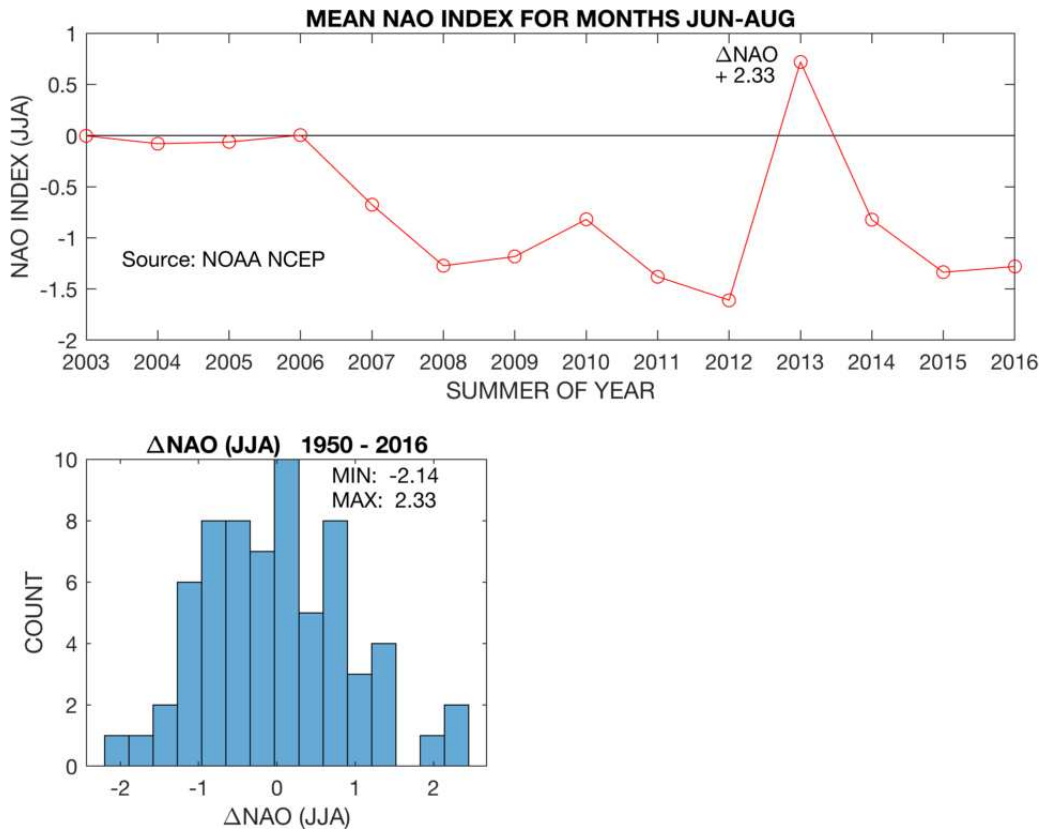


Figure S7. (a) the summertime NAO index for June-Aug (NAO JJA) for years 2003–2016, and (b) the distribution of all inter-annual changes in this index from 1950–2016. As seen previously with the NAO JJAS index (Fig. 1) the magnitude of the index change between 2012 and 2013 was the largest ever observed.

6. Surface Mass Balance (SMB) Modeling

We used version 3.5.2 of the regional climate model called Modèle Atmosphérique Régional (MAR) (Fettweis et al., 2013b), extensively and successfully validated over Greenland (Fettweis et al., 2017), to estimate the SMB trend shown in Fig 5c. The reanalysis ERA-Interim is used for 6 hourly forcing of MAR's lateral boundaries. MAR comprises a high resolution, regional climate model that simulates atmospheric processes coupled with the Soil Ice Snow Vegetation Transfer (SISVAT) scheme, dealing with surface and sub-surface processes, which incorporates the multilayer snow/firn/ice energy balance model CROCUS. We refer to Fettweis et al. (2013b, 2017) for a more detailed description of MAR.

We have also examined the SMB time series produced by the regional climate model RACMO2 (i.e. version 2.3p2) which combines the dynamical core of the numerical weather model HIRLAM with the European Center for Medium Range Weather Forecasting (ECMWF) Integrated Forecast System (IFS) physics. Like MAR, RACMO2 is forced at its lateral domain boundaries using the 6-hourly fields of ERA-Interim. We utilized monthly averaged SMB fields obtained on a 1 km grid which was downscaled from a 5.5 km grid. See ref. (5) and <https://www.projects.science.uu.nl/iceclimate/models/racmo.php> for more details about RACMO2.

We have integrated the SMB fields over Greenland as a whole (i.e. including both the GrIS and the outlying ice caps), and computed SMB over the summers (JJA and JJAS) of 2003 through 2016. In Fig.1f we compare the summertime SMB (JJAS) computed using MAR and RACMO2 with the summertime NOA index (JJAS). This provides additional evidence that the decadal acceleration and the abrupt deceleration in mass loss, inferred from GRACE (Fig. 1), mostly manifested summertime SMB changes tied to the phase of the summertime NAO. (A similar result is found if we use the JJA definition for summertime). The change in summertime SMB (JJAS) from 2012 to 2013 was +439 GT according to MAR, and +355 GT according to RACMO2. This discrepancy is consistent with the rule of thumb fairly widely adopted by numerical weather modelers working on Greenland, the SMB estimates have error levels (mostly driven by biases) of the order of ~ 10 %.

We took a much longer view of SMB in Fig. 5e where we showed that the cumulative mass changes driven only by SMB, when integrated over all Greenland, were remarkably steady

between 1980 and about 2002. The average rate of change of cumulative SMB found using MAR was about 434.5 GT/yr. In Fig. S8 we show the results of a similar computation based on RACMO2, and this extends the cumulative SMB time series back to 1958. The degree of agreement between the cumulative SMB rates through 2002 computed from the RACMO2 predictions (437.2 Gt/yr) and from MAR (434.5 Gt/yr) is probably fortuitous, but even so, this result (**Fig. S8**) gives considerable additional support to our suggestion (Fig 5e) that in terms of SMB, a critical threshold was passed near the turn of this millennium.

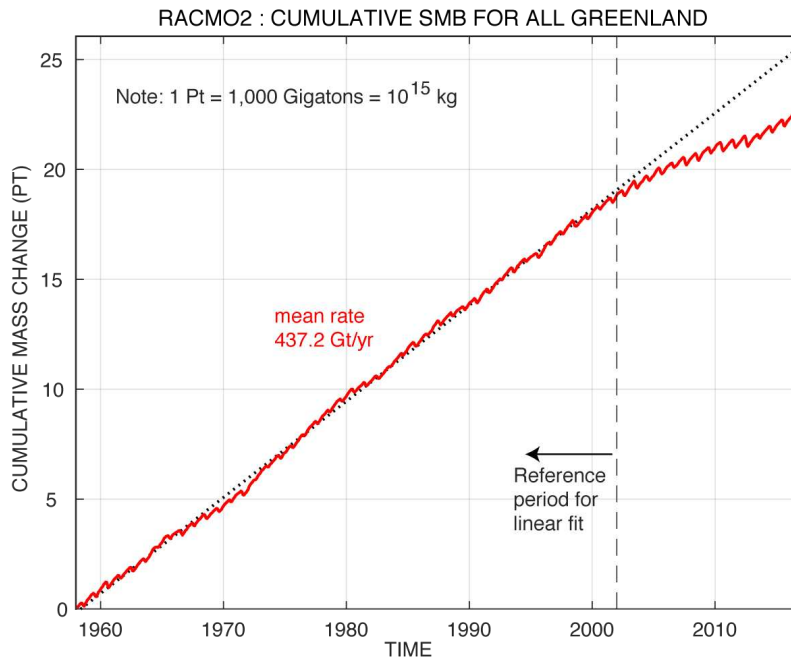


Figure S8. Cumulative mass changes due to SMB, integrated over Greenland, from RACMO2.

7. Jakobshavn Glacier as a center of accelerating mass loss in West Central Greenland

We showed in the main text that the sustained mass acceleration recorded by GRACE from 2003-2012 was quite strongly focused in SW Greenland, a region nearly devoid of marine-terminating outlet glaciers, and so we inferred this acceleration was largely driven by changing SMB. That is, we claim that south of 68.5° N and west of about 45° W the mass acceleration field seen in Fig. 5a was dominated by negative trends in SMB. This zone does not include Jakobshavn Glacier (JG), also known as Jakobshavn Isbrae, where increases in discharge rate have driven dynamic thinning of the GrIS between latitudes of about 68.7° N and 69.5° N (10). Nielsen et al. (10)

studied four GNET stations in this sector, including station KAGA, located very close to the calving front of JG. They showed that three quarters of the uplift at KAGA, prior to the summer of 2010, was driven by ice loss centered near the frontal portion of the JG. In contrast station ILUL, further west, sensed slightly more ice loss away from JG's ice loss center than near it. Uplift at stations QEQE and AASI much further to the west, and therefore most sensitive to long wavelength loading, was dominated by mass loss well outside of the JG ice loss center. Ref. (10) also documented an acceleration in uplift rates from 2006-2010 to 2010-2012, and suggested that SMB changes drove at least one third of this acceleration, even at KAGA. In Figure S9 below, we update the time series for KAGA which has the strongest sensitivity to dynamic ice loss by virtue to its proximity to the zone of active thinning (see Fig. 1 in ref. 36). If we fit the displacement time series at KAGA using a quadratic or 'constant acceleration' trend (plus an annual cycle) we find that uplift accelerated from 2007.36 through 2013.4 at a mean rate of 3.9 ± 0.9 mm/yr², with vertical velocity increasing from about 11 mm/yr to about 34 mm/y. In order to search for a possible change in acceleration rate prior to 2013.4, we refit the time series using a cubic trend model, which allows acceleration to change linearly as a function of time. The best fit model (**Fig. S9**) has an acceleration rate which increases with time, consistent with the suggestion of Nielsen et al. (10) that increased runoff in the summers of 2010 and 2012 contributed to the observed acceleration in mass loss.

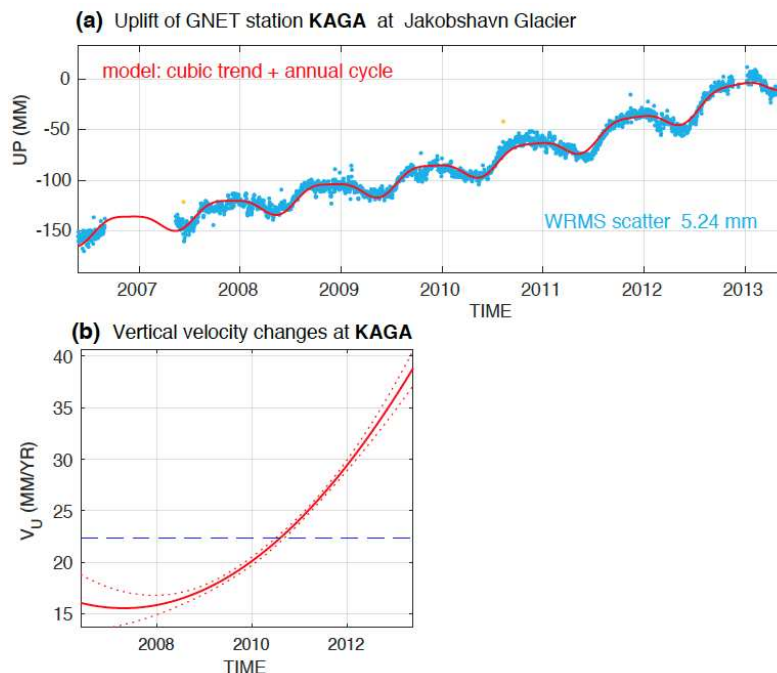


Figure S9. (a) uplift and (b) uplift rate at GNET station KAGA modeled using a trajectory model consisting of an annual cycle superimposed on a cubic trend.

The newly published results of King et al. (32) provide us with a more direct way to assess the contribution of DMB or discharge trends to the mass acceleration field observed by GRACE near JG, and further south. They show (in their Fig. S3 a) a strong positive trend in discharge at JG between the beginning of 2000 and late 2006, implying a negative acceleration in ice mass of roughly -2.1 Gt/yr^2 . But they also show almost no trend in discharge at JG between late 2006 and early 2012. No trend in discharge means no trend in DMB, and therefore no DMB-driven acceleration in ice mass in this nearly 5-year period of time. We conclude that the sustained acceleration in ice mass observed by GRACE in West Central Greenland was probably dominated by shifting DMB at JG prior to late 2006, but from 2007 to early 2012, the acceleration recorded by GRACE was dominantly due to a strong negative trend in SMB.

It is interesting to note that the discharge at JG did increase substantially during the summer of 2012, when summertime melting peaked just prior to the Pause, and then decayed rather slowly during the following three years, suggesting that the dynamical behavior of JB was perturbed for several years by the major melting anomaly of 2012.

The results obtained by ref. (32) also pertain to the mass acceleration further south, in SW Greenland, where there are only two significant outlet glaciers over a very large section of the ice margin. The largest of these is Kangiata Nunaata Sermia (KNS) and the other is Narsap Sermia. King et al. (32) showed (in their Fig. 3a) that the cumulative discharge of all SW Greenland glaciers, including KNS and NS, was remarkably constant from 2000 to 2016, with a mean discharge close to 9.5 Gt/year . There was a weak temporal trend to regional discharge, but it was a decline, implying a *positive* mass acceleration of order $\sim 0.1 \text{ Gt/yr}^2$. We conclude that the strong negative mass accelerations sensed by GRACE and GNET in SW Greenland were almost entirely driven by SMB.

8. A second way to characterize the mass anomaly field associated with the Pause

In the main text, we visualized the mass anomaly associated with the Pause by examining the difference between the projected mass loss trajectory model and the GRACE solution at epoch 2014.45 (Fig. 5 b). Alternatively, we can average the mass anomalies in the interval 2013.79-2014.45 just as we did in Fig. 1d, but now as a function of position (**Fig. S10**: this is the average of the last 8 frames in our mass anomaly movie).

The most obvious difference between Figs. 5b and S10 is the presence of an isolated, roughly circular negative anomaly (colored yellow) located in central East Greenland, within the GrIS. The anomaly has a peak value of ~ 121 mm w.e. and most of the mass anomaly resides in a disk of diameter ~ 300 km. Given that GRACE's spatial resolution is ~ 334 km, we clearly cannot infer the true spatial extent of this mass fluctuation, should it be real. The anomaly started to develop towards the end of our reference period, beginning by 2013.46, and it was last clearly present at 2014.29. This enigmatic anomaly is developed over high interior ice and cannot plausibly be explained in terms of a SMB anomaly or glacier dynamics. If it was precipitated by a subglacial lake drainage event (29, and Howat et al., 2015), the total volume of water expelled would have to be ~ 7 km³, or rather more, which is far larger than the volume of any subglacial lake so far identified in Greenland, or even hypothesized (Livingstone et al., 2013). Unless the draining subglacial lake or lakes have a very large total area (say $> 10,000$ km²) then related surface subsidence should be easily detectable using repeat altimetry, should it be available. If surface subsidence is not detected, our only other explanations are an unusually persistent artifact (Velicogna and Wahr, 2013) in the underlying GRACE solutions, or some kind of Gibbs phenomenon associated with spectral truncation.

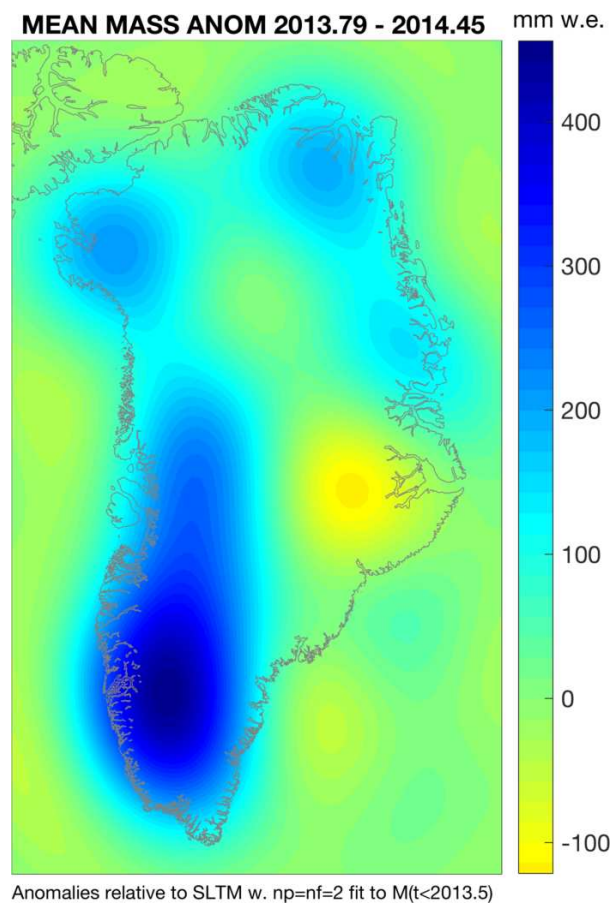


Figure S10. The spatial distribution of the mean mass anomaly in the time window 2013.79–2014.45, which corresponds to the last 8 frames of the mass anomaly movie. This result is fairly similar to the last mass anomaly field (the last frame of our mass anomaly movie) depicted in Fig. 5b.

9. The Influence of GrIS Topography on Surface Temperature

In the main text, we argued that the influence of atmospheric warming is strongly modulated in space by ice surface elevation (Fig. 5d). In **Fig. S11** we see the mean surface temperature of the GrIS in May, averaged over the interval 1980–1999, as inferred by the regional climate model MAR. Very little of the ice surface is even close to the melting point, and virtually none has reached it. As the summer develops, melting will begin in the south and move north, and it will start at the lowest elevations (near the edges of the ice sheet) and migrate upwards (towards the interior of the ice sheet). Examine the 2 km ASL contour in Fig S11, and also at Fig. 5d, and note how in any modest range of latitudes, surface elevation strongly influences the surface temperature in May, prior to the onset of summer, and therefore strongly influences the amplitude of the temperature increase required, at any given location, to initiate surface melting. A 5°C increase in surface temperature will cause a larger area (per unit margin length) of melting in SW Greenland where the 2 km contour is most distant from the ice margin, than it will much further south in SE Greenland, where the 2 km contour lies very much closer to the ice margin. And a 5° C increase in central E Greenland will cause a much smaller area of surface melting than the same increase will produce in central W Greenland. What is true of seasonal warming is also true of the enhanced transient warming associated with a strongly negative phase of the summertime NAO, and for the secular increase in summertime temperatures associated with global warming. Indeed, we have argued that it was the *combined* impact of progressive global warming and transient warming (and higher insolation) that triggered the unprecedented (Fig. 5e and Fig. S8, ref. 31) and accelerating SMB-induced mass loss between 2003 through 2012, which at its peak in the summer of 2012 actually caused the entire ice sheet surface to melt for a short period of time, even at the highest parts of the ice sheet. When the ‘collaboration’ between global warming and NAO ceased for 12-18 months starting in 2013, it no surface melting occurred at any great height.

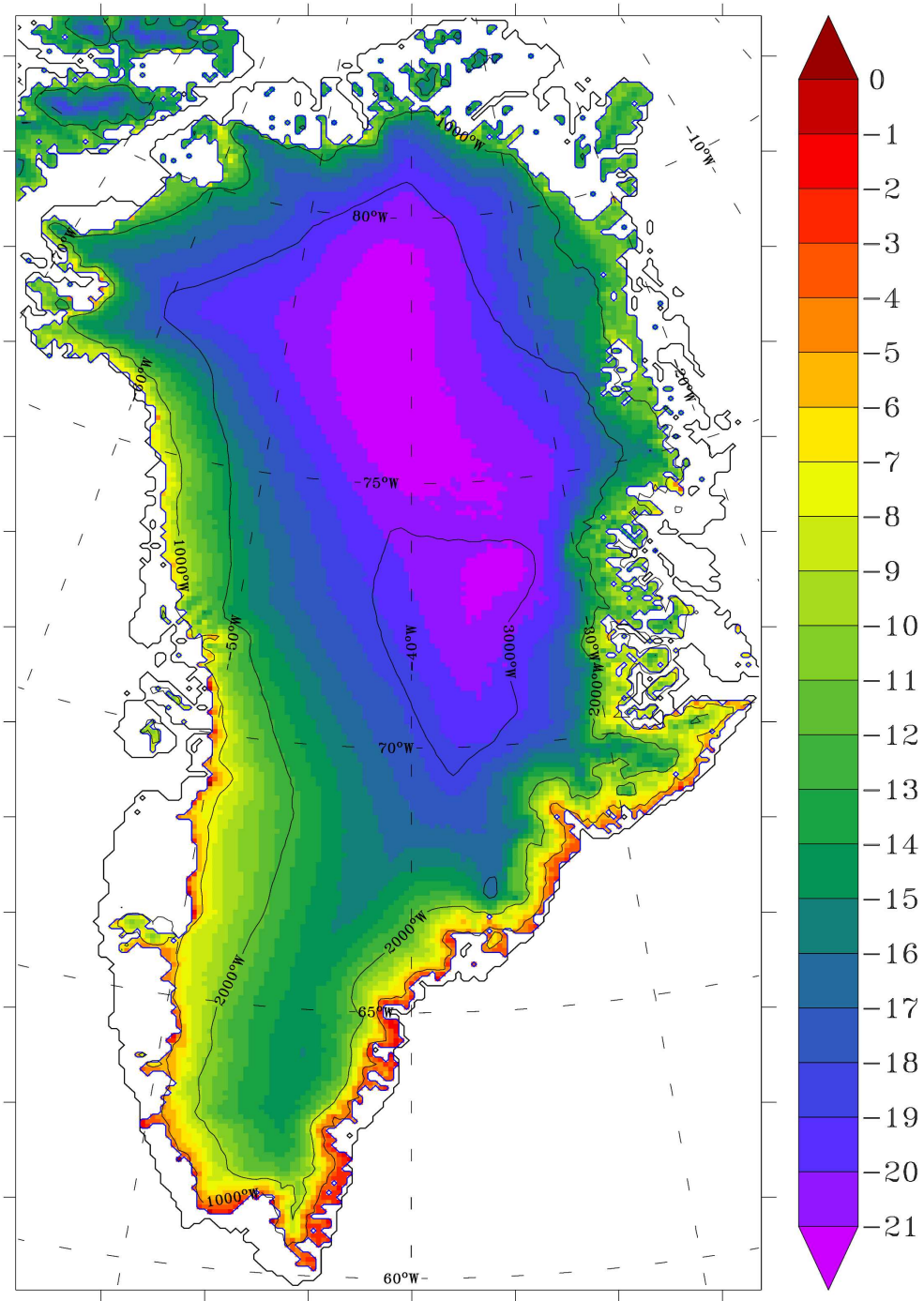


Figure S11. The mean surface temperature of the GrIS in May during the 20 year time interval 1980 – 1999, as computed by the numerical weather model MAR at 10 km resolution. Only the very edges of the ice sheet are even close to the melting point (0°C), and even these areas are confined to southern Greenland.

10. The Atlantic Multidecadal Oscillation (AMO)

It is well established that increases in glacial discharge in Greenland have been driven in significant part by warming of shallow ocean waters (Luckman et al., 2006; and refs. 33,34). Ocean warming is driven by progressive global warming and by natural cycles such as the ENSO and, of more relevance to Greenland, the Atlantic Multidecadal Oscillation (AMO) (Howat et al., 2008; Hanna et al, 2013). But could sea surface temperature (SST) fluctuations associated with the AMO have contributed to the intense but spatially focused mass accelerations recorded by GRACE and by GNET? We address this question using the AMO index produced by NOAA, which can be found at <https://www.esrl.noaa.gov/psd/data/correlation/amon.us.data> and <https://www.esrl.noaa.gov/psd/data/correlation/amon.us.long.data> We plot the summertime values of this index, at different time scales, in **Fig. S12**.

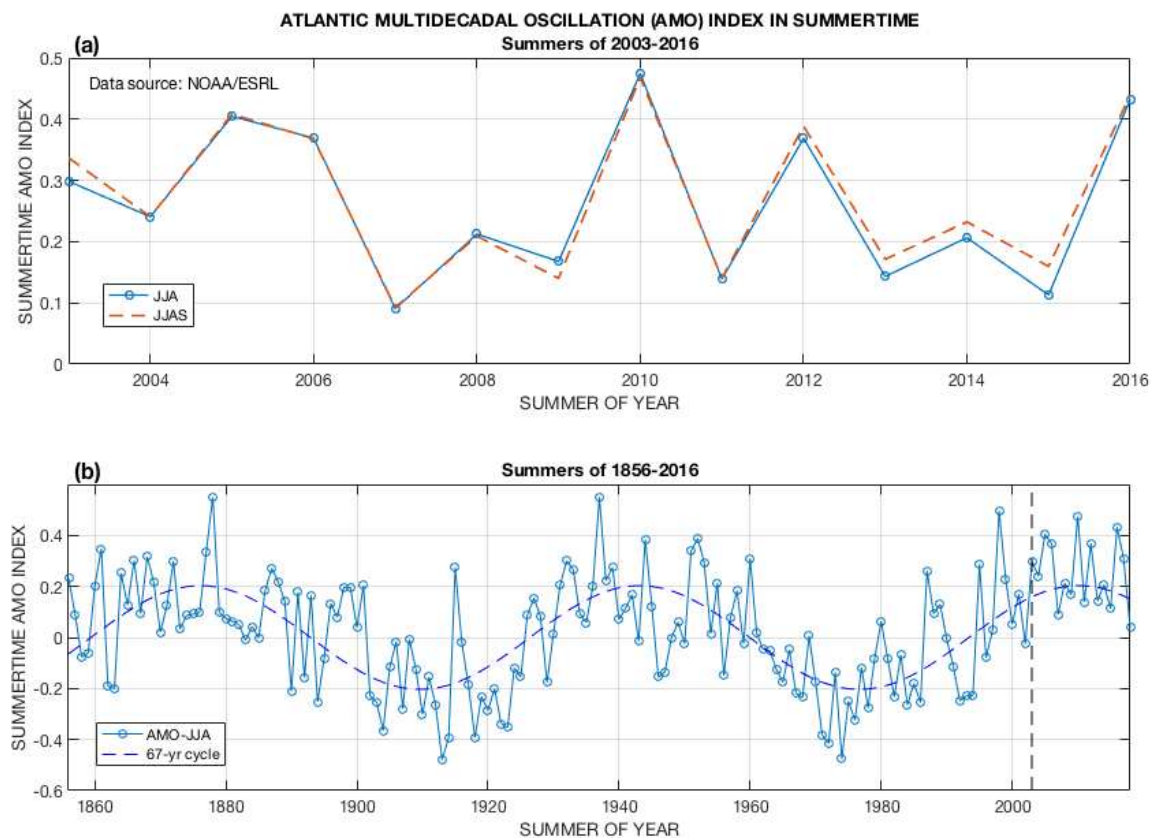


Fig. S12 (a) The summertime AMO index (JJA and JJAS) for the summers of 2003 - 2016. (b) The summertime AMO index (JJA) from 1856 to 2016 and the best fitting sinusoid, with a period of 67 years.

We saw, in Fig. 1f, a striking correlation between the sNAO index and summertime SMB in Greenland. This correlation is consistent with the ~ 10 year acceleration in mass loss recorded by GRACE, and its nearly complete reversal during the Pause, which began in the summer of 2013. In Fig. S12 (a) we show the summertime AMO index in the same general time period, and there is no similarity in its behavior. A positive shift in AMO has the same ‘warming’ influence as a negative shift in the summertime NAO. There is no sustained upwards trend in the AMO from 2003 through 2012, nor is there an unusually large jump, in the opposite direction, in the summer of 2013.

This is not very surprising when we examine the structure of the AMO from 1856 to present (Fig. S12 b). The dominant periodicity is about 67 years, and as such the AMO could hardly be responsible for the enormous change that developed between the summers of 2012 and 2013. There is no compelling reason to believe that the summertime AMO had a significant influence on the sustained (~ 10 -year) mass loss acceleration recorded by GRACE immediately prior to the Pause. What the second plot does reveal is that the positive temperature fluctuations codified by the AMO were reinforcing global ocean warming from the early 1980’s to about 2003-2005, but subsequently the AMO curve was essentially stalled close to its maximum value or turning point, and soon its influence will reverse, and AMO will tend to oppose global ocean warming for 2-3 decades.

11. Tipping Points: An Analogy with Coral Bleaching

We have argued that the increasingly negative summertime phase of the NAO in the 6-year period that culminated in the summer of 2012 was a major driver of the unprecedented acceleration in ice loss recorded by GRACE prior to 2013. Earlier sustained downward shifts of the sNAO index did not achieve similar accelerations in ice loss because, during the last century, the air was too cold for such transient increases in temperature and insolation to trigger greatly increased melting and runoff. There is an interesting analogy with the El Niño–Southern Oscillation (ENSO) quasi-cycle and the phenomenon of coral bleaching (Williams and Bunkley-Williams, 1990; Glynn, 1991; Goreau and Hayes, 1994; Brown et al., 1996; Huppert and Stone, 1998; Hoegh-Guldberg, 1999; Hughes et al., 2003; 2018).

Although multiple factors contribute to coral bleaching, including changes in salinity, sedimentation, pollution, bacterial infection, ocean acidification, and overfishing, it is now well

established that the major cause of coral bleaching is thermal stress due to ocean warming, and that the ENSO cycle has had an erratic, but powerful and recurring influence on coral bleaching (Goreau and Hayes, 1994; Huppert and Stone, 1998; Hughes et al., 2018). Coral bleaching events were both rare and highly localized prior to 1960. The first regional coral bleaching event occurred in 1980. The hypothesis that major, non-localized bleaching events were associated with the positive sea surface temperature (SST) perturbations driven by El Niño events became firmly established by the early 1990s, and has been confirmed by all subsequent experience. The first ‘global’ or pan-tropical bleaching event was triggered by the El Niño event of 1997/98, which was then the strongest El Niño event on record. The second global coral bleaching event (GCBE) was triggered by the El Niño event of 2010. It lasted less than 1 year, and was recognized as the 2nd worst bleaching event on record. The third, longest, most widespread and most destructive GCBE, lasted from mid 2014 to mid 2017.

El Niño events produce pulses of shallow ocean warming, so the recent association between El Niño events and coral bleaching is easily understood. But why is this association so recently established? Why were GCBEs not occurring the 19th or the early and mid 20th century? El Niño events, and the pulses of warming associated with El Niño events, have occurred for many centuries, and probably for millennia, but since the mid 20th century the successive pulses have been superimposed on rather more steady and progressive SST increases driven by global warming. Thus, the peak temperatures driven by El Niño events have tended to peak higher and higher as time progressed. In 1980 the peak was high enough to thermally stress corals and trigger bleaching at a regional level. But 1997/98 the threshold temperature for bleaching was crossed over a large fraction of the tropical and sub-tropical oceans. By the time of the 2014-2017 event, the ‘background’ ocean temperature had risen to the extent that the El Niño could cause very large areas of shallow water to warm well beyond the bleaching threshold for nearly all shallow water corals. Sadly, the long-term prospects for coral reef ecosystems is one of massive if not total extinction.

The analogy we wish to draw is fairly obvious. The positive summertime temperature and insolation fluctuations associated with the negative phase of the NAO did not cause truly major negative shifts in SMB in the last century just as El Niño events did not cause GCBEs until the late 1990’s. But just as progressive global ocean warming has enabled the ENSO to trigger coral bleaching events of unprecedented scale and intensity, the progressive increases in atmospheric temperature driven by the enhanced greenhouse effect have enabled the fluctuations tied to the

NAO to trigger unprecedented levels of melting and runoff over large parts of the Greenland ice sheet (Fig. 5 e,g).

The NAO forms part of the Arctic Oscillation, but neither phenomenon is truly cyclical in the sense of having a well-defined periodicity. The NAO need not spend equal amounts of time in its positive and negative phases. There has been some speculation that global warming could encourage the NAO to spend more time in its negative phase (e.g. Jaiser et al., 2012; Francis and Vavrus, 2012 and ref. 14). Based on our analysis, this would enhance the pace of Greenland's deglaciation. Even if this speculation is incorrect, continued global warming implies that whenever the sNAO index becomes strongly negative in the future we can expect progressively more negative shifts in SMB. Even more worrying is that it is only a matter of time, perhaps just a decade or two, before global warming will bring Greenland summers that are warmer than the summer of 2012, even when the NAO is in its neutral or positive phase. And in another 30 years or so, the AMO will begin, once again, to reinforce global ocean warming. All these factors should be taken into account when we assess future acceleration in the rate of sea level rise (Nerem et al., 2018), and the impact that increased seawater freshening may have on the stability of the ocean circulation system (Thornally et al., 2018).

It is very likely that the acceleration in total glacial discharge that occurred in the 1990s also arose due to a 'collaboration', rather like that between global warming and the NAO, but in this case between global ocean warming and the AMO. The AMO tracks sea surface temperature, so in the 1990's, rising AMO (Fig. S12b) reinforced ocean warming to the extent that the combined warming drove a significant acceleration in total glacial discharge that could be documented in many parts of Greenland by the year 2000 (ref. 32). But by 2003 -2005 this collaboration had effectively ended (at a high point) and now the AMO is falling (Fig. S2b), and thus working against the impacts of global ocean warming.

12. Data Availability

The GRACE solutions used in this study can be downloaded from the Center for Space Research at <http://www2.csr.utexas.edu/grace/RL05.html> . The (Slepian filtered) mass grid time series is available as a Matlab data cube, on request from Michael Bevis. The GNET GPS data used in this study can be downloaded in RINEX format from the UNAVCO, Inc. data archive at

<https://www.unavco.org/data/gps-gnss/data-access-methods/dai2/app/dai2.html#> or can be obtained from the DTU Space Institute by sending a request to S. Abbas Khan (abbas@space.dtu.dk). Daily coordinate time series for GNET stations are available from the Nevada Geodetic Laboratory, see <http://geodesy.unr.edu/NGLStationPages/GlobalStationList>. The MAR SMB grids can be obtained from Xavier Fettweis (xavier.fettweis@ulg.ac.be) on request. The RACMO2 SMB results can be obtained from Michiel van den Broeke (M.R.vandenBroeke@uu.nl) on request. NOAA's monthly NAO indices can be found here: <http://www.cpc.ncep.noaa.gov/products/precip/CWlink/pna/nao.shtml>

A Microsoft PowerPoint file containing movies of our seasonally-adjusted GRACE mass change solutions, and related quantities, is available on request from Michael Bevis (mbevis@osu.edu).

13. Additional References

- Bevis M., A. Brown and E. Kendrick (2012) Devising stable geometrical reference frames for use in geodetic studies of vertical crustal motion, *Journal of Geodesy*, **87**, 311-321, doi: 10.1007/s00190-012-0600-5.
- Brown. B., R. Dunne and H. Chansang (1996) Coral bleaching relative to elevated seawater temperature in the Andaman Sea (Indian Ocean) over the last 50 years. *Coral Reefs*, **15**, 151-152.
- Francis, J. A., and S. J. Vavrus (2012), Evidence linking Arctic amplification to extreme weather in mid-latitudes, *Geophys. Res. Lett.*, **39**, L06801, doi:10.1029/2012GL051000
- Glynn, P. (1991) Coral reef bleaching in the 1930s and possible connections with global warming, *Trends in Ecology and Evolution*, **6**, 175-179.
- Goreau, T. and R. Hayes (1994) Coral bleaching and ocean 'hot spots', *Ambio*, **23**, 176-180.
- Hoegh-Guldberg, O. (1999) Climate change, coral bleaching and the future of the world's coral reefs, *Marine Freshwater Research*, **50**, 839-66.
- Hanna, E., J. Jones, J. Cappelen, S. Mernild, L. Wood, K. Steffen and P. Huybrechts (2103) The influence of North Atlantic atmospheric and oceanic forcing effects on 1900 -2010 Greenland summer climate and ice melt/runoff, *International Journal of Climatology*, **33**, 862-880.
- Howat, I., I. Joughlin, M. Fahnestock, B. Smith and T. Scambos (2008) Synchronous retreat and acceleration of southern Greenland outlet glaciers 2006 – 2006: ice dynamics and coupling to climate, *Journal of Glaciology*, **54**, 646-660.
- Howat, I., C. Porter, M. Noh, B. Smith, and S. Jeong (2014) Brief Communication: Sudden drainage of a subglacial lake beneath the Greenland Ice Sheet, *Cryosphere*, **9**, 103–108, doi:10.5194/tc-9-103-2015
- Hughes, T. et al. (2003) Climate change, human impact and the resilience of coral reefs, *Science*, **301**, 929-933.

- Hughes, T. et al. (2018) Spatial and temporal patterns of mass bleaching of corals in the Anthropocene, *Science*, **359**, 80 – 83.
- Huppert, A. and L. Stone, (1998) Chaos in the Pacific's coral reef bleaching cycle, *American Naturalist*, **152**, 447 – 459.
- Jaiser, R., K. Dethloff, D. Handorf, A. Rinke, and J. Cohen (2012), Impact of sea ice cover changes on the Northern Hemisphere atmospheric winter circulation, *Tellus*, **64**, 11595, doi:10.3402/tellusa.v64i0.11595
- Livingstone S., C. Clark, J. Woodward, and J. Kingslake (2013) Potential subglacial lake locations and meltwater drainage pathways beneath the Antarctic and Greenland ice sheets, *Cryosphere*, **7**, 1721–1740, doi:10.5194/tc-7-1721-2013
- Luckman, A., T. Murray, R. de Lange, and E. Hanna (2006) Rapid and synchronous ice-dynamic changes in East Greenland, *Geophysical Research Letters*, **33**, L03503, doi:10.1029/2005GL025428.
- Nerem, S., B. Beckley, J. Fasullo, B. Hamilton, D. Masters and G. Mitchum, 2018, Climate-change-driven accelerated sea-level rise detected in the altimeter era, *Proc. Nat. Acad. Sci.* , www.pnas.org/cgi/doi/10.1073/pnas.1717312115
- Thornally, D., D. Oppo, P. Ortega, J. Robson, C. Brierly, R. Davis, I. Hall, P. Moffa-Sanchez, N. Rose, P. Spooner, I. Yashayaev and L. Keigwin, 2018, Anomalously weak Labrador Sea convection and Atlantic overturning during the past 150 years. *Nature*, **556**, 227 – 230.
- Velicogna, I. and J. Wahr (2013) Time-variable gravity observations of ice sheet mass balance: Precision and limitations of the GRACE satellite data, *Geophys. Res. Lett.*, **40**, 3055-3063, doi:10.1002/grl.50527
- Williams, E. and L. Bunkly-Williams (1990) The world-wide coral reef bleaching cycle and related sources of coral mortality, *Atoll Research Bulletin*, **335**, 1 – 71.